Direct measurement of the effective charge in nonpolar suspensions by optical tracking of single particles

G. Seth Roberts,[1] Tiffany A. Wood,[1] William J. Frith,[2] and Paul Bartlett[1,*]

[1] *School of Chemistry, University of Bristol, Bristol BS8 1TS, UK.*
[2] *Unilever Research Colworth, Colworth House, Sharnbrook, Bedford MK44 1LQ, UK.*

(Dated: Revision: 1.15, January 20, 2007, 14:59:21 (UTC))

We demonstrate a novel technique for the measurement of the charge carried by a colloidal particle. The technique uses the phenomenon of the resonance of a particle held in an optical tweezers trap and driven by a sinusoidal electric field. The trapped particle forms a strongly damped harmonic oscillator whose fluctuations are a function of γ, the ratio of the root-mean square average of the electric and thermal forces on the particle. At low applied fields, where $\gamma \ll 1$, the particle is confined to the optical axis while at high fields ($\gamma \gg 1$) the probability distribution of the particle is double-peaked. The periodically-modulated thermal fluctuations are measured with nanometer sensitivity using an interferometric position detector. Charges, as low as a few elementary charges, can be measured with an uncertainty of about 0.25 e. This is significantly better than previous techniques and opens up new possibilities for the study of nonpolar suspensions.

I. INTRODUCTION

Although charge is often thought to play no role in nonpolar media there is ample [1, 2, 3], if sometimes contradictory [4], evidence of surface charging in nonpolar colloidal suspensions. Much of the reason for this uncertainty is the extremely low level of charge in nonpolar environments. While a particle of radius $a \sim 500$ nm might carry a surface charge eZ_{eff} of the order of 10^3 electrons in an aqueous dispersion ($\epsilon_r \sim 80$), the charge in a nonpolar solvent will be some two or three orders of magnitude smaller. Although small in absolute terms, this charge still produces surprisingly strong effects in low dielectric environments. For instance, using Coulomb's law the contact value of the interaction potential (in units of k_BT) between two colloidal spheres with radius a and charge eZ_{eff} in a solvent of dielectric ratio ϵ_r is simply,

$$\frac{U_0}{k_BT} = \frac{1}{k_BT} \cdot \frac{Z_{\text{eff}}^2 e^2}{8\pi\epsilon_0\epsilon_r a} = \left(\frac{\lambda_B}{2a}\right) Z_{\text{eff}}^2, \qquad (1)$$

where we have introduced the Bjerrum length $\lambda_B = e^2/4\pi\epsilon_0\epsilon_r k_BT$ as a characteristic length scale of electrostatic interactions. For dodecane, λ_B is 28.0 nm so the repulsive interactions between 500 nm particles, carrying a typical charge of 10 electrons, is $\approx 3\ k_BT$ – big enough to have a dramatic effect on the structure of a colloidal suspension.

The most direct route to monitor the extent of particle charging is to measure the uniform drift velocity u_D in the presence of a weak electric field E. For a spherical particle, $u_D = \mu E$, where μ is the electrophoretic mobility. For an isolated colloidal sphere, in the low-salt regime, moving in a solvent of viscosity η, Stokes' law implies $\mu = Z_{\text{eff}}e/(6\pi\eta a)$ since the ionic atmosphere around the colloid is very diffuse. The low charges found in nonpolar media therefore translate to electrophoretic mobilities some two or three orders of magnitude or so less than in water, at the same electric field. Rapid and reproducible measurements of such low mobilities presents a major challenge to conventional electrokinetic techniques [1].

Motivated by the growing acknowledgement of the importance of charge in nonpolar suspensions [5] and its technological significance [6], several novel methods have been developed to determine particle mobility in nonpolar suspensions. Schätzel and coworkers [7] pioneered an innovative amplitude-weighted phase analysis signal processing scheme for the analysis of classical laser Doppler electrophoresis data. The technique, phase analysis light scattering (PALS), is significantly more sensitive than conventional laser Doppler electrophoresis. In practice however, collective particle motion induced by thermal convection or sedimentation restricts the achievable sensitivity of commercial PALS instruments to $\sim 10^{-10}$ m^2 s^{-1} V^{-1}, which corresponds to colloid charges of $\sim 10e$ on a particle of radius $a = 500$ nm. Video microscopy has been used by several authors. Perez and Lemaire [8] used a vibrating piezoelectric stage to null the oscillatory microscopic motion produced by an applied alternating field, while Strubbe et al. [9] have measured the diffusion constant and electrophoretic mobility of individual particles in a nonpolar suspension. Despite these developments there is still no technique which can provide fast and accurate measurement of the extremely small levels of particle charge found in nonpolar suspensions. As a result the microscopic charging mechanisms in non-aqueous media has remained largely problematic [4]. Improvements in quantitative characterization are an essential first step to developing a more detailed understanding of the role of charge in nonpolar suspensions.

In this paper, we present a simple technique that allows a direct measurement of the effective charge of colloidal particles in nonpolar solvents. Our approach is

*Electronic address: p.bartlett@bristol.ac.uk

very different from standard electrophoretic light scattering methods and uses the phenomenon of the driven resonance of a strongly-damped harmonic oscillator. We use the radiation pressure from a laser beam focused to a near diffraction-limit spot (an 'optical tweezer') to trap single colloidal particles in a dilute suspension. The focused beam produces a harmonic potential for the trapped particle whose strength is proportional to the laser power. The hindered diffusion of the trapped colloid is modified by an oscillatory electric field. The modulated thermal fluctuations are measured with nanometer sensitivity and the charge extracted from the spectral density of the fluctuations at the field frequency.

Our approach is similar in principle to the classical Millikan oil drop experiments [10] but uses light rather than gravity. In his famous experiment to prove the quantization of charge, Millikan measured the speed of a charged oil drop under gravity and its speed falling in a electric field E. He switched on electric forces $F_E = ZeE$ of between 300–1300 fN (1 fN = 10^{-15}N) on oil drops with radii between 2 and 6 μm (each drop containing Z elementary charges, e) to counterbalance the gravitational force mg acting on the drop. Our experiments rely, instead, on using the random thermal forces leading to Brownian motion, to oppose an applied electric force. The balance of forces determines the diffusive motion of the particle, rather than the velocity of free-fall as in Mullikan's experiment. Below we demonstrate that, by using a weak optical trap and an interferometric position detection system, we can measure accurately a mean particle charge of -2.9 e which, for the typical field strengths used, corresponds to an electric force of about 40 fN. We estimate that the sensitivity of our technique is about an order of magnitude smaller than this limit. We believe our method is a significant improvement on existing techniques. It provides rapid, accurate and highly sensitive information on the status of particle charging in nonpolar suspensions. Related but less sensitive experiments have been described on highly-charged aqueous colloids by Garbow et al. [11] where the authors used a weakly-focused laser beam. This had the effect of pushing particles along the optical axis, rather than stably confining them, as in our approach.

This paper is organized as follows: After a description of the apparatus and measurement procedures, we give a short introduction to the theory of a driven overdamped harmonic oscillator before results obtained on a variety of different nonpolar suspensions are presented and discussed in the final section.

II. MATERIALS AND METHODS

A. Materials.

We use a model non-aqueous colloidal system of sterically-stabilized poly(methyl methacrylate) spheres of radius $a = 610 \pm 30$ nm suspended in dodecane. The particles were synthesized by dispersion polymerization, following the procedures detailed by Antl et al. [12]. Electron microscopy revealed the particles were highly uniform in size with a radius polydispersity (root mean square variation / mean radius) of $\sigma = 0.046 \pm 0.01$. Dodecane was dried with activated molecular sieves (Acros, size 4A) and stored under dry nitrogen. Sodium bis(2-ethylhexyl) sulfosuccinate (NaAOT, Fluka BioChemika Ultra 99%) was purified by dissolution in methanol and tumbled with activated charcoal. Zirconyl 2-ethyl hexanoate [$Zr(Oct)_2$] was purchased from Alfa Aesar (Heysham, UK) and used as received.

B. Optical Tweezers.

Figure 1 shows a schematic of our optical tweezer system. A fibre-coupled laser beam with wavelength $\lambda = 1064$ nm (Ytterbium fiber laser, IPG Photonics, Germany) was focussed to a diffraction-limited beam waist by a microscope objective (Plan-Neofluar, ×100, N.A. 1.3, Zeiss) mounted in an inverted microscope (Axiovert S100, Zeiss). The laser intensity ($\sim$ 10 mW) was varied using a $\lambda/2$ waveplate and a polarizing beam-splitter cube placed in the beam path. The fluctuations in position of the trapped particle, with respect to the center of the trap, were measured with a quadrant photodetector (model QD50-4X, Centronics, UK) using back-plane optical interferometry [13]. The particle positions were acquired by a Labview programme (National Instruments, Austin, Texas, USA) and digitized using a high-speed data acquisition card (National Instruments model PCI-MI0-16E-1) at 10 kHz. For the current experiments, the number of particle positions collected in each time trace was set at 2^{18}, so that the duration of each measurement was $\approx$ 26 s. Positions measured in voltages were converted into displacements in nanometers by recording the time-dependent mean-square displacement $\langle \Delta x^2(\tau) \rangle$ of five particles from the same batch of particles, immediately before each set of electrophoresis measurements. The laboratory temperature was stabilized at 22 $\pm$ 1 °C. At this temperature the viscosity of dodecane is 1.378 x 10^{-3} Pa s and the dielectric constant is 2.002.

C. Single Particle Optical Microelectrophoresis (SPOM).

The microelectrophoresis cell was constructed from two platinum foil electrodes, 127 μm high and with a width of 2 mm, mounted in a cylindrical glass sample chamber, 1.13 mm high with a volume of $\sim$ 90 μl. The cell was constructed in three stages. First, two platinum foil electrodes were carefully positioned parallel to each other onto a 5.0 cm x 2.5 cm rectangular glass coverslip (170 μm thick), covered with a thick layer of a UV-activated glue (Loctite 350), using a low-magnification stereo microscope. The electrodes were securely fixed in

place by irradiation with a 100 W UV-lamp. Then a 1 mm thick glass slide with an 1 cm diameter inset circular hole was placed on top of the electrodes and sealed to the electrodes with UV glue. Finally, immediately prior to use, the top of the chamber was closed by a 22 mm diameter 170 μm-thick circular coverslip. The use of optical quality cover-slips on both the bottom and top of the sample chamber minimized spherical abberation.

The distance between the two electrodes was measured, after assembly of the cell, using a calibrated microscope graticule as 128 μm $\pm$ 2μm. The small gap between the electrodes makes it possible to generate electric fields on the order of tens of kilovolts per meter with just a few volts applied to the cell, which minimizes thermal instabilities due to Joule heating and avoids the electrohydrodynamic fluid instabilities which occur at higher voltages [14]. The electric field was estimated from the expression $E = \lambda V/d$, where V is the applied voltage, d is the plate separation and, λ is a factor correcting for the finite size of the electrodes. Analytical calculations [15], for the field on the midplane equidistant between two semi-infinite plates, give $\lambda = 0.969$ for the rectangular electrodes used. Accumulation of ions near the electrode and the generation of a non-uniform space charge was suppressed by using an ac voltage. Electrosmosis was minimized by positioning the electrodes 60 μm above the bottom glass wall, so that the tangential electric field at the wall was reduced. Moving the position of the trapped particle away from the electrode center by 10 μm, in any direction, changed the recorded charge by less than 2.5%, confirming the absence of electrosmotic fluid flows.

The sample chamber was filled with a dilute suspension of colloidal particles with a volume fraction of $\sim 10^{-5}$. The cell was carefully centered so that the laser passed through a plane equidistant between the two electrodes and the focus was midway between the top and bottom surfaces. The particle was held at least 65 μm from the nearest surface, to ensure Stokes' law was applicable. The charge on the particle was analysed using a purpose-written software package written in IDL (Research Systems, Boulder, Colorado). The sign was determined by reducing the frequency of the applied electric field to 0.5 Hz, blocking the laser beam so that the particle was momentarily released from the optical trap, and following the oscillatory motion of the free particle on a CCD camera.

The accuracy of SPOM was checked by measuring the mobility of a 850 nm (radius) PMMA particle in dodecane (with 100 mM NaAOT) using a commercial PALS instrument (Brookhaven ZetaPlus), $\mu_{\rm PALS}$, and the SPOM technique, $\mu_{\rm SPOM}$. The good agreement between $\mu_{\rm SPOM}$ ($(-5.4\pm\ 0.5)$ x 10^{-10} m^2 s^{-1} V^{-1}) and $\mu_{\rm PALS}$ ($(-6.0\pm\ 0.5)$ x 10^{-10} m^2 s^{-1} V^{-1}) confirms that the optical microelectrophoresis technique yields accurate particle mobility data.

III. THEORY

A colloidal particle illuminated by a laser beam encounters a gradient force that is oriented in the direction of the intensity gradient and a scattering force that is oriented in the direction of the incident light. In a tightly-focused beam the gradient forces dominate and lead to a strong restoring force, which causes the particle to be confined near the focus of the beam. To a first approximation, the particle can be modeled as a mass m in a three-dimensional harmonic potential. The potential is characterized by two spring constants, one in the axial and one in the radial direction. Here, for simplicity, we analyze only the one-dimensional motion along the radial coordinate x, where the corresponding force constant is k_H.

Placed in an external electric field, the total force on a *charged* particle is a sum of three contributions: a harmonic force, $-k_H x(t)$, arising from the optical trap; a random force $\mathcal{R}(t)$ that represents thermal forces at the temperature T; and an external periodic force $F_p(t) = A\sin(\omega_p t + \phi)$ which is characterized by the frequency ω_p, amplitude A and initial phase ϕ of the external field. Defining the effective charge on the particle as $Z_{\rm eff}$ (in units of the fundamental charge e) then the amplitude of the oscillatory force is

$$A = Z_{\rm eff} eE, \tag{2}$$

where E is the maximum electric field strength at the particle center. In a single particle optical microelectrophoresis experiment, the quantity ultimately measured is the time-dependent particle autocorrelation function $C(\tau)$, or its Fourier-transform, the spectral density $I(\Omega)$. Below we derive expressions for both quantities, in terms of the effective charge $Z_{\rm eff}$.

A. A periodically-driven Brownian Oscillator

The fluctuations of a periodically-driven Brownian oscillator are described, in the conventional Ornstein-Uhlenbeck theory [16], by the Langevin equation

$$m\ddot{x}(t) + \xi\dot{x}(t) + k_H x(t) = A\sin(\omega_p t + \phi) + \mathcal{R}(t). \tag{3}$$

Here $x(t)$ is the particle trajectory, and $\xi = 6\pi\eta a$ is the friction coefficient of a sphere of radius a moving in a medium of viscosity η. The random thermal forces are modeled by a Gaussian process $\mathcal{R}(t)$ with the moments,

$$\langle\mathcal{R}(t)\rangle = 0, \qquad \text{and} \qquad \langle\mathcal{R}(t)\mathcal{R}(t')\rangle = 2\xi k_B T\delta(t-t'). \tag{4}$$

This definition ensures that the Brownian particle is in thermal equilibrium at a temperature T, in the absence of any driving field i.e. for $A = 0$.

A colloidal particle, once moving, loses momentum rapidly as a result of viscous losses. The characteristic time for this decay is $t_B = m/\xi$, which is about

10^3 times smaller than the time resolution of our experiments, when digitizing at a 10kHz sampling rate. Consequently the inertial terms may safely be dropped so that Eq. 3 now reads

$$\xi\dot{x}(t) + k_H x(t) = A\sin(\omega_p t + \phi) + \mathcal{R}(t). \quad (5)$$

The equation is linear so that the general solution may be written [17],

$$x(t) = x_n(t) + x_p(t), \quad (6)$$

where x_n is the solution in the presence of random thermal forces *only* (i.e. $A = 0$) and x_p is the solution when only periodic forces act (i.e. $T = 0$). We now consider each solution in turn.

The driven oscillator is deterministic in the absence of any random thermal noise. The solution is well known [17],

$$x_p(t) = \frac{A}{k_H\left[1 + (\omega_p/\omega_c)^2\right]^{1/2}}\sin(\omega_p t + \phi - \Delta). \quad (7)$$

The particle motion lags the driving field by a constant phase factor,

$$\Delta = \tan^{-1}\frac{\omega_p}{\omega_c}, \quad (8)$$

which varies with the relative sizes of the driving and the *corner frequency*,

$$\omega_c = k_H/\xi. \quad (9)$$

The frequency ratio ω_p/ω_c also controls the amplitude of the particle motion. For low frequencies ($\omega_p \ll \omega_c$), the amplitude is essentially frequency independent. While, at high frequencies ($\omega_p \gg \omega_c$) the response decreases rapidly with increasing ω_p. In between, Eq. 7 reveals a monotonic oscillation spectrum, without the dynamic resonance at $\omega_p = \omega_c$, characteristic of underdamped systems. The relative phase of the particle motion depends on the initial phase ϕ of the applied force. In our experiments ϕ is a fluctuating stochastic variable with a coherence time τ_p, which depends on the stability of the voltage generator. The phase is essentially randomized on times $t \gg \tau_p$ so time and phase averages are equivalent. Multiplying the trajectories at t and t' and averaging over ϕ, assuming the initial value of ϕ is uniformly distributed over the interval $[0, 2\pi]$, yields the correlation function,

$$\langle x_p(t)x_p(t')\rangle_\phi = \frac{A^2}{2k_H^2\left[1 + (\omega_p/\omega_c)^2\right]}\cos\omega_p(t - t'), \quad (10)$$

where the subscript denotes the phase-averaging. Since the motion is totally deterministic, $\langle x_p(t)x_p(t')\rangle_\phi$ oscillates continuously between positive and negative values.

The dynamics of the trapped particle is a linear superposition of periodic and random motion. The correlation function of a purely Brownian oscillator is given by Doi and Edwards [18] as,

$$\langle x_n(\tau)x_n(0)\rangle_\mathcal{R} = \frac{k_B T}{k_H}\exp(-\omega_c\tau). \quad (11)$$

The mean-square displacement is accordingly $\langle x_n^2\rangle_\mathcal{R} = k_B T/k_H$ and, since $F = -k_H x$, the mean-square thermal forces on the trapped particle are $\langle F_n^2\rangle_\mathcal{R} = k_B T k_H$.

B. Correlation function and spectral density

The correlation function $c(\tau)$ of the periodically-driven Brownian oscillator is defined by

$$c(\tau = t' - t) = \langle\langle x(t)x(t')\rangle_\mathcal{R}\rangle_\phi, \quad (12)$$

where the averages are taken over both noise and phase. Since the thermal and periodic forces are uncorrelated, $c(\tau)$ is simply a sum of the correlation functions for periodic and purely thermal motion,

$$c(\tau) = \frac{k_B T}{k_H}\exp(-\omega_c\tau) + \frac{A^2}{2k_H^2\left[1 + (\omega_p/\omega_c)^2\right]}\cos\omega_p\tau. \quad (13)$$

It is more convenient to work with the normalized function $C(\tau) = c(\tau)/c(0)$, which may be written as

$$C(\tau) = \frac{1}{1+\gamma^2}\exp(-\omega_c\tau) + \frac{\gamma^2}{1+\gamma^2}\cos\omega_p\tau, \quad (14)$$

where we have introduced γ^2, the scaled *ratio of the mean-square periodic and Brownian forces*,

$$\gamma^2 = \frac{\langle F_p^2\rangle / \langle F_n^2\rangle}{1 + (\omega_p/\omega_c)^2}. \quad (15)$$

Here $\langle F_p^2\rangle = Z_{\text{eff}}^2 e^2 E^2/2$ and $\langle F_n^2\rangle = k_B T k_H$. The force ratio γ appears naturally in the theory of a driven Brownian oscillator and, as we show below, is also the quantity most readily extracted from experiment. Knowing γ, the charge on the particle follows immediately as,

$$e|Z_{\text{eff}}| = \frac{\gamma\xi}{E}\sqrt{\frac{2k_B T}{k_H}(\omega_p^2 + \omega_c^2)}. \quad (16)$$

This expression simplifies at low frequencies ($\omega_p \ll \omega_c$) to,

$$e|Z_{\text{eff}}| = \frac{\gamma}{E}\sqrt{2k_B T k_H} \quad (17)$$

which does not depend on the radius of the trapped particle.

Figure 3 shows the force ratio γ calculated for typical experimental parameters. In the weak-field limit, where $\gamma \ll 1$, the motion of the trapped particle is dominated by random thermal forces. By contrast, in the strong-field limit where $\gamma \gg 1$, the thermal forces are only a relatively small perturbation and the electrophoretic forces

dominate. The cross-over between these two regimes occurs at a particle charge of $Z_{\text{eff}} \sim 20$, for typical field strengths. At this point the electric forces on the particle are a few hundred femtonewtons.

The force ratio γ may be determined experimentally from the correlation function $C(\tau)$ or, equivalently, from the spectral density,

$$I(\Omega) = \frac{1}{2\pi}\int_{-\infty}^{\infty} c(\tau)\exp(-i\Omega\tau)d\tau. \tag{18}$$

As we discuss below there are advantages to both approaches. Inserting Eq. 13 into 18 reveals that the spectral density is a sum of two independent contributions,

$$I(\Omega) = \frac{k_B T}{\pi\xi}\frac{1}{\Omega^2+\omega_c^2} + \frac{k_B T\gamma^2}{2k_H}[\delta(\Omega-\omega_p)+\delta(\Omega+\omega_p)], \tag{19}$$

a Lorentzian spectrum typical of Brownian motion in a harmonic potential, together with additional δ-spikes at the positive and negative field frequencies. Integrating the spikes over the frequency axis gives an expression for the mean-squared periodic displacement of the particle P_{sig},

$$P_{sig} = \int_{-\infty}^{\infty} I_p(\Omega)d\Omega = \frac{k_B T}{k_H}\gamma^2. \tag{20}$$

from which γ can be found.

C. Asymptotic probability distribution function

We now turn to the probability distribution of the confined particle. Introducing the dimensionless position coordinate $\bar{x} = x/(k_B T/k_H)^{1/2}$, we define the probability of locating the Brownian particle in the region between $\bar{x}$ and $\bar{x}+d\bar{x}$ as $p(\bar{x})d\bar{x}$, where $p(\bar{x})$ is the probability distribution function.

Without a periodic force, the Brownian particle is at thermal equilibrium and $\bar{x}(t)$ follows the Boltzmann's distribution,

$$p_n(\bar{x}) = \frac{1}{\sqrt{2\pi}}\exp(-\bar{x}^2/2). \tag{21}$$

Applying a time-dependent force perturbs the system and shifts the average distribution away from the equilibrium result. When all transients have died out, the probability approaches a new asymptotic distribution which is a periodic function of the time t. As discussed earlier, the only experimentally accessible quantities are the phase-averaged functions. Analytical expressions for the phase-averaged distributions have been proposed by Jung and Hänggi [19], for arbitrary friction coefficients. In the overdamped limit, their result reduces to the infinite series,

$$p(\bar{x}) = \frac{1}{\sqrt{2\pi}}\exp\left(-\frac{\bar{x}^2+\gamma^2}{2}\right)\left\{I_0\left(\frac{\gamma^2}{2}\right)I_0\left(\sqrt{2}\gamma\bar{x}\right) + 2\sum_{k=1}^{\infty}(-1)^k I_k\left(\frac{\gamma^2}{2}\right)I_{2k}\left(\sqrt{2}\gamma\bar{x}\right)\right\} \tag{22}$$

where $I_k(x)$ is a modified Bessel function [20]. Figure 4 shows the effect of a finite external field on the probability distribution. With increasing amplitude, the probability $p(\bar{x})$ first broadens until, at $\gamma = \gamma^*$, the distribution becomes bimodal and develops two peaks around $\bar{x} \sim \pm\,\gamma$. Further increases in the external field lead the two peaks to split further apart, leaving a relatively flat distribution around the origin, as the particle becomes increasingly localized around the two extremities.

The changes in the probability distribution with external field can be clearly seen from the curvature of $p(\bar{x})$ near to the origin. Expanding Eq. 22 around $\bar{x} = 0$ gives, to terms in $\bar{x}^2$,

$$p(\bar{x}) = \frac{1}{\sqrt{2\pi}}\exp\left(-\frac{\gamma^2}{2}\right)I_0\left(\frac{\gamma^2}{2}\right)(1-\kappa\bar{x}^2) \tag{23}$$

where the curvature is

$$\kappa = \frac{1}{2}\left[1-\gamma^2+\gamma^2\frac{I_1(\gamma^2/2)}{I_0(\gamma^2/2)}\right]. \tag{24}$$

κ is positive for a single monomodal distribution and negative for a bimodal distribution. The inset plot in Fig. 4 displays the variation of κ with external field. The curvature first decreases rapidly with increasing γ, reflecting the broadening of $p(\bar{x})$ evident at low modulation strengths, before changing sign for $\gamma > \gamma^* = 1.257$ as the distribution becomes bimodal. The small negative values of the curvature found at high fields correspond to the extremely flat shape of the distribution seen close to the origin at high γ. The curvature is a function solely of γ^2 so that the distribution sharpens continuously with increasing frequency and does not show the resonant bimodality evident in the underdamped limit [19].

The width of the particle distribution is $\langle x^2\rangle$, which from Eq. 13, equals

$$\langle x^2\rangle = \frac{k_B T}{k_H}(1+\gamma^2) \tag{25}$$

where $\langle\cdots\rangle$ denotes an average over both $\mathcal{R}$ and ϕ. In the weak-field limit where $\gamma \ll 1$, the width of the dis-

tribution approaches the thermal limit, k_BT/k_H. Broadening of the probability distribution is only significant in the strong-field limit ($\gamma \gg 1$) where the width varies quadratically with the strength of the applied field.

IV. RESULTS AND DISCUSSION

A. Field and Frequency Dependence of Effective Charge

To validate our technique, experiments were first carried out on a number of weakly-charged particles, as a function of the applied field strength and its frequency. The particles were taken from a dilute dispersion of 610 nm (radius) poly(methyl methacrylate) particles in a 0.035 wt% solution of a PHSA-g-PMMA copolymer in dodecane. Figure 5 shows a short portion of the x- and y-position of a trapped particle when a sinusoidal field is applied. The field was applied along the x-axis so periodic oscillations are expected in the x-signal and should be absent from the y-signal. Looking at the trajectories plotted in Fig. 5, it is very difficult to see any significant differences between the x- and y-signals. The small electrophoretic oscillations expected are 'buried' beneath much larger Brownian fluctuations and $\gamma \ll 1$. To extract the small periodic excursions from the predominantly random Brownian motion we determine the spectral distribution of the fluctuations.

Figure 6 shows the normalized autocorrelation functions, $C(\tau)$, measured on the same particle, as the applied field was varied. The oscillatory component is clearly visible, particularly at long times. Data collection is fast with each of the functions shown representing just 26 s worth of data. The alternating electric field had a frequency of 67 Hz and voltages of up to 10 V were applied to the electrodes. The laser trap had a stiffness of $k_H = 4.7 \pm 0.1$ fN nm^{-1} and a corner frequency of 47 ± 1 Hz. The agreement between the experimental data and the least-squares fits is excellent. Fig. 6(a) reveals that at short-times the correlation functions all essentially converge, even though their long time dependence is clearly very different. This is because on timescales shorter then the period of the applied field, the motion of the trapped particle is dominated by Brownian diffusion. Thermal fluctuations are independent of the field and, since they are uncorrelated, result in the exponential relaxation apparent at short times in $C(\tau)$ (Eq. 11). The oscillations evident at long times (Fig. 6(b)) reflect the periodic motion produced by the applied field and accordingly grow as the applied field is increased.

Fitting the measured correlation functions to the theoretical expression for $C(\tau)$ (Eq. 14) yields γ, the ratio of the rms electrophoretic and Brownian forces. The ratio is plotted in Figure 7 as a function of the applied field E. As expected, the experimental values of γ are linearly proportional to E, confirming that the charge on the particle is constant. The gradient of the plot yields an effective charge of $|Z_{\text{eff}}| = 14.5 \pm 0.2\ e$, equivalent to an electrophoretic mobility of $\mu = 1.46 \pm 0.02$ x 10^{-10} m^2 s^{-1} V^{-1}. The charge on this particle is sufficiently low that, even at the maximum field strengths achievable, the system remains in the low-field limit ($\gamma < 1$) where Brownian forces dominate.

For ultra-low charges where $\gamma \ll 1$ it becomes increasingly difficult to determine the oscillatory element in the autocorrelation function, because of fluctuations in the baseline. This can be seen in the data at 13.3 kV m^{-1} in Figure 6(b) where the oscillations are indistinct. To resolve these low particle charges we perform a fast Fourier transform of the data and calculate the spectral density. Figure 8 shows the field dependence of the resulting power spectra. The measured spectra are particularly simple, being a superposition of a Lorentzian spectrum (shown dashed) reflecting diffusive motion and a single δ-peak at the fundamental electrode drive frequency ω_p, whose height increases with the applied field. The data contains no higher harmonics of ω_p confirming the linear response of particle and field. To extract the power in the periodic signal, the data around the δ-spike was masked and the diffusive spectrum fitted to the first term of Eq. 19, by adjusting the unknown corner frequency ω_c. Subtracting the fitted Lorentzian from the measured power spectra yielded the signal spectrum. The mean-square electrophoretic displacement P_{sig} was obtained by integrating the signal spectrum around the peak at ω_p. The resulting values for P_{sig} are plotted as a function of the square of the applied field, in the inset of Figure 8. As expected from Eq. 20, the mean-square displacement P_{sig} varies linearly with E^2. The high positional sensitivity achievable is highlighted by the arrowed δ-peak in Fig. 8 which, while it remains clearly visible, corresponds to a mean-square displacement of only 1.4 nm^2.

To explore how the frequency of the applied field influenced the measurements we collected autocorrelations at a number of different field frequencies, taking care to ensure that the same particle was used in each case. The corner frequency of the trapped particle was $\omega_c = 291$ rad s^{-1} and data was recorded at frequencies between 25 rad s^{-1} and 1930 rad s^{-1}, approximately an order of magnitude below and above the corner frequency of the optical trap. The amplitude of the applied field was fixed at 75.8 kV m^{-1}. The autocorrelations were analyzed as described above to determine γ^2 at each frequency. The results are summarized in Figure 9. As expected, from the discussion in III A, the response of the trapped particle to the applied field decreases with increasing frequency. This drop in sensitivity is particularly sharp when the driving frequency exceeds the corner frequency of the optical trap. Plotting γ^2 as a function of the frequency ratio $1 + (\omega_p/\omega_c)^2$ confirms that γ^2 is inversely dependent on $1+(\omega_p/\omega_c)^2$, in agreement with the predictions of Eq. 15. The highly linear dependency evident in Fig. 9 confirms the validity of the driven harmonic model and indicates that the charge on the particle is frequency independent. Analysis gives the surface charge on the

particle as $|Z_{\rm eff}| = 15.8 \pm 0.2$.

B. Field Dependence of Probability Distribution Function

So far, we have found excellent agreement between our measurements and the theoretical predictions for a periodically-driven oscillator. The comparison has however been limited to weakly-charged particles where $\gamma < 1$. To extend our understanding, we now look at more highly-charged particles where strong electrophoretic forces dominate the weaker Brownian forces. Hsu et al. has shown [3] that non-polar suspensions may be charged by adding the surfactant, sodium bis(2-ethylhexyl) sulfosuccinate (Na-AOT), which forms reverse micelles in a non-polar solvent. Adding Na-AOT to our suspensions at concentrations of 100 mM increases the average charge (in electrons) on the PMMA particles by a factor of four to $Z_{\rm eff} \approx -50$. Using these more highly-charged particles we are able to investigate the high-field limit where $\gamma > 1$.

Figure 10 shows the field dependence of the particle probability. The normalized distribution function is plotted as a function of the dimensionless position $\bar{x} = x/(k_BT/k_H)^{1/2}$, where the x-location of the sphere has been scaled by the size of the corresponding *rms* Brownian fluctuations in the optical trap. To correct for small asymmetries in the trap caused by optical misalignment, the measured probability was averaged together at each positive and negative displacement. The resulting symmetrized distributions, $p_s(\bar{x}) = [p(\bar{x}) + p(-\bar{x})]/2$, are plotted in Figure 10. At zero field the probability distribution is a simple Gaussian function, as expected from Eq. 21. Increasing the field to $E \approx 23$ kV m^{-1} causes the distribution to broaden, although it remains singly-peaked. At fields of 46 kV m^{-1} and above there is a dramatic change in $p_s(\bar{x})$. The central peak in the distribution first splits into two broad maxima, before then moving further apart in $\bar{x}$ as the field is increased still further. Using the experimentally-determined charge on the particle ($Z_{\rm eff} = -48.3 \pm 0.3$) and the measured optical trap stiffness we calculate the force ratio γ from the applied electric field E. In this way we have confirmed that the probability distribution first becomes bimodal at a force ratio in the range $1.01 < \gamma < 1.34$. This observation is in good agreement with the theoretical predictions of Section III C where a bimodal distribution is predicted for $\gamma > \gamma^* = 1.257$.

To account for the dramatic changes evident in the measured distributions we have calculated $p(\bar{x})$ for a periodically-driven oscillator. The exact shape of this distribution depends solely upon the force ratio γ, as noted in Section III C. Fixing γ at the experimental value, we have evaluated numerically the series of Bessel functions given in Eq. 23. The infinite series was truncated when convergence to four significant figures was achieved. The results of these calculations are plotted as the solid lines in Figure 10. The agreement is remarkably good and is particularly encouraging given that there are no adjustable parameters in the comparison.

C. Sensitivity Limit

The smallest charge that can be detected by our technique is fixed by the point where the peak in the spectral density at ω_p (the arrowed peak in Fig. 8) becomes indistinguishable from the Brownian background. At this point the spectral power in a band of width $\Delta\omega$ centred on ω_p is $P_{sig} = \Delta\omega \cdot (k_BT/\pi\xi)/(\omega_c^2 + \omega_p^2)$. The corresponding ratio of electric to Brownian forces is $\gamma^2 = \Delta\omega \cdot \omega_c/\pi(\omega_c^2 + \omega_p^2)$ and the smallest detectable particle charge is therefore,

$$e|Z_{\rm eff}^{\rm min}| = \frac{\sqrt{12 k_B T \eta a \Delta\omega}}{E} \tag{26}$$

where we have used Eq. 20. In a discrete Fourier transform the minimum width $\Delta\omega$ of a frequency channel is determined by the total time t_0 of data acquisition and equals, $\Delta\omega = 2\pi/t_0$. In our system where $a = 610$ nm, $\eta = 1.38$ mPa s, and the maximum field strength is $E \sim 80$ kV m^{-1}, the minimum detectable charge is about 0.25 e for an experimental run of $t_0 = 26$ s. This is equivalent to a limiting electrophoretic mobility of $\sim 2.5 \times 10^{-12}$ m^2 V^{-1} s^{-1}.

D. Measurement of Charge Distributions

We have shown that optical microelectrophoresis provides an accurate, rapid and highly sensitive determination of the effective charge on an individual trapped particle. In many cases, of course, the population from which the single particle is selected is heterogeneous. There is a distribution of particle charges which reflects, for instance, the stochastic nature of the charging mechanism or variations in the surface chemistry or the size of individual particles. Many of the conventional methods used to probe the electrokinetics of colloidal suspensions (microelectrophoresis, laser Doppler electrophoresis, and electroacoustics) only allow for the calculation of the average mobility. They provide either little or no information on the distribution of particle charges. In many cases, however, knowledge of the charge distribution is of vital importance. Colloidal suspensions have, for example, proved to be valuable model systems in condensed matter physics. There is strong evidence that the width of the charge distribution (the charge polydispersity) significantly influences the glass transition and at high levels may suppress the freezing transition in these systems [21]. It is therefore important that techniques are available which allow an accurate characterization of the charge distribution.

We consider a suspension of colloidal particles with (effective) charges Ze which are distributed according to a

normalized charge distribution function $P(Z)$. The mean charge and charge polydispersity σ_Z are defined by

$$\overline{Z} = \int_0^\infty P(Z) Z \mathrm{dZ} \quad (27)$$

$$\sigma_Z = \frac{1}{\mid \overline{Z} \mid} \left(\int_0^\infty P(Z)(Z - \overline{Z})^2 \right)^{1/2}. \quad (28)$$

To characterize the charge distribution we trap and measure the effective charge of 50–100 individual particles. Although a little tedious these repeated measurements are still quick. For instance it takes a couple of minutes per particle to manually measure its charge: 20–30 s scanning time to locate a particle, a short delay of 30 s to center the particle trap and a further 30 s for data collection.

To explore the range of applicability and resolution of the technique we determined the charge distribution in nonpolar suspensions of PHSA-coated PMMA spheres. These colloidal spheres have been widely used in fundamental studies of nucleation, crystallization and glass formation since the coating with PHSA is thought to provide a hard-sphere type interaction. Figure 11(a) shows the charge distribution measured for PHSA-coated PMMA spheres suspended in clean dry dodecane. Clearly the particles are very weakly charged, with an average colloidal charge of just three electrons per sphere, equivalent to an electrophoretic mobility of $\mu = -3 \times 10^{-11}$ m^2 s^{-1} V^{-1} and a zeta potential of -3.5 mV. Indeed the particle mobility was sufficiently small to be undetectable on a commercial PALS instrument. The low mobilities however presented no problems for the optical microelectrophoresis measurements, as the data in Figure 11(a) confirms. Although the charge on the PHSA-coated spheres is small, it is clearly non-zero and so we expect a weak, soft repulsion between the particles. To gauge the level of this repulsion we estimate the average contact value U_0 of the interaction potential between spheres. An average charge of $\overline{Z} = -2.9$ equates to a value of $U_0/k_BT = 0.2$ in dodecane (Eq. 1). Although the value is small in comparison to thermal energies it can not be ignored in quantitative studies. This is highlighted by, for instance, the recent studies of Auer et al. [22] who have explored the effect of a very similarly-sized weak repulsion on the crystallization rate. They found that soft spheres crystallize some two orders of magnitude faster than a comparable system of pure hard spheres. Clearly, for quantitative studies, it is important to fully characterize the interaction potential and optical microelectrophoresis offers a promising alternative to existing techniques.

The data in Figure 11(a) reveals a second distinctive feature. The suspension is amphoteric, in that it contains both positive and negatively-charged spheres. Close to two-thirds of the particles are negative and the remainder positive. While the charge distribution seems to be approximately Gaussian in shape, the width is broad with a charge polydispersity of $\sigma_Z = 1.5 \pm 0.3$, which is surprisingly large.

As a further example of the applicability of the optical electrophoresis method, Figure 11(b) and (c) show the effect of adding the surfactants, $Zr(Oct)_2$ [b] and Na-AOT [c], at concentrations of 2 mM to dilute PMMA suspensions in dodecane. These surfactants form reverse micelles in nonpolar solvents such as dodecane. A finite fraction of these micelles spontaneously ionize at room temperature [23]. Particles then acquire charge either by preferentially adsorbing the micelles of one sign or by the dissociation of a surface group, with the subsequent ionic species being solubilized within a reverse micelle. While the micelle-mediated charging of colloids has been known for at least the last 60 years [4], the exact mechanism of charging in nonpolar media remains problematic and is not well understood. Figure 11 reveals that addition of $Zr(Oct)_2$ causes the PMMA spheres to become strongly positively charged, while Na-AOT generates a large negative particle charge. Using the Hückel equation [24] we calculate the equivalent zeta potentials to be +63 mV for the $Zr(Oct)_2$ treated spheres and -60 mV for the AOT containing suspensions. A comparable value for the zeta potential of around -38 mV was found by Kihara et al. [25] for PMMA particles in cyclohexane with added AOT. While Hsu et al. [3] observed significantly higher zeta potentials, of around -140 mV for PMMA in dodecane. In the case of $Zr(Oct)_2$, data is more limited, although Croucher et al. [26] reports that poly(vinyl acetate) particles are charged positive by the zirconyl salt. Surprisingly, we find that the charge distribution of the zirconyl and AOT suspensions are very sharply peaked with charge polydispersities of 5.0 ± 0.5% for the AOT system and 5.8 ± 0.6% for ZrOEH. In both cases the charge polydispersities are comparable, allowing for the sampling errors, to the size polydispersity of the colloid (4.6 ± 1%). Detailed information on the charging mechanism in these systems will be published elsewhere.

V. CONCLUSIONS

In summary, we have demonstrated a novel technique for the direct measurement of small colloid charges commonly found in nonpolar suspensions. The charge is measured by confining an individual particle to a harmonic optical potential and by following the excitation of the particle by a sinusoidal electric field. The trapped particle forms a strongly damped oscillator. By using a weak optical trap and an interferometric position detector we have shown that single particle optical microelectrophoresis (SPOM) is capable of very high sensitivity. Surface charges on the level of a few elementary charges can be detected on individual colloidal particles, with an uncertainty of about 0.25 e. Other techniques of measuring the charge on a particle are generally less sensitive. Our measurements are rapid and reproducible, with data on a single particle being recorded in approximately 30 s. When applied to multiple particles our technique yields

information on the distribution of particle charges rather than simply recording the average charge, as provided by most conventional electrokinetic techniques. These characteristics makes SPOM ideal for the characterization of nonpolar suspensions and may prove useful to study fundamental phenomena in colloid chemistry, such as the relaxation of the double layer. For example, one might be able to detect discrete changes in the charge on a particle, due to the time-dependent relaxation of the double layer. Work exploring these possibilities is currently underway.

Acknowledgments

The authors wish to thank Unilever for partial funding and for permission to publish these results. Support from the UK Engineering and Physical Sciences Research Council is gratefully acknowledged. Adele Donovan is thanked for help with particle synthesis and Kirsty Paul for PALS measurements.

[1] R. E. Kornbrekke, I. D. Morrison, and T. Oja, Langmuir **8**, 1211 (1992).
[2] W. H. Briscoe and R. G. Horn, Langmuir **18**, 3945 (2002); R. I. Keir, Suparno, and J. C. Thomas, Langmuir **18**, 1463 (2002); J. C. Thomas, B. J. Crosby, R. I. Keir, and K. L. Hanton, Langmuir **18**, 4243 (2002); C. E. McNamee, Y. Tsujii, and M. Matsumoto, Langmuir **20**, 1791 (2004); P. G. Smith, W. Ryoo, and K. P. Johnston, J. Phys. Chem. B **109**, 20155 (2005).
[3] M. F. Hsu, E. R. Dufresne, and D. A. Weitz, Langmuir **21**, 4881 (2005).
[4] I. D. Morrison, Coll. Surf. **71**, 1 (1993).
[5] P. Royall, M. E. Leunissen, and A. van Blaaderen, J. Phys.: Condens. Matter **15**, S3581 (2003); M. E. Leunissen, C. G. Christova, A.-P. Hynninen, C. P. Royall, A. I. Campbell, A. Imhof, M. Dijkstra, R. v. Roij, and A. v. Blaaderen, Nature **437**, 235 (2005); P. Bartlett and A. I. Campbell, Phys. Rev. Lett. **95**, 128302 (2005).
[6] B. Comiskey, J. D. Albert, H. Yoshizawa, and J. Jacobson, Nature **394**, 253 (1998); Y. Chen, J. Au, P. Kazlas, A. Ritenour, H. Gates, and M. McCreary, Nature **423**, 136 (2003); S. A. Jones, G. P. Martin, and M. B. Brown, J. Pharm. Sci. **95**, 1060 (2006).
[7] K. Schatzel and J. Merz, J. Chem. Phys. **81**, 2482 (1984); J. F. Miller, K. Schatzel, and B. Vincent, J. Coll. Interf. Sci. **143**, 532 (1991).
[8] A. T. Perez and E. Lemaire, J. Coll. Interf. Sci. **279**, 259 (2004).
[9] F. Strubbe, F. Beunis, and K. Neyts, J. Coll. Interf. Sci. **301**, 302 (2006).
[10] R. A. Millikan, Phys. Rev. **32**, 349 (1911).
[11] N. Garbow, M. Evers, and T. Palberg, Coll. Surf. A **195**, 227 (2001).
[12] L. Antl, J. W. Goodwin, R. D. Hill, R. H. Ottewill, S. M. Owens, S. Papworth, and J. A. Waters, Colloids Surf. **17**, 67 (1986).
[13] F. Gittes and C. F. Schmidt, Opt. Lett. **23**, 7 (1998).
[14] V. J. Novotny, in *Colloids and Surfaces in Reprographic Technology: ACS Symposium Series*, edited by M. L. Hair and M. D. Croucher (American Chemical Society, Washington DC, 1982), vol. 200, pp. 281–306.
[15] P. Morse and H. Feshbach, *Methods of Theoretical Physics, Vol II* (McGraw-Hill, 1953).
[16] G. E. Uhlenbeck and L. S. Ornstein, Phys. Rev. **36**, 823 (1930).
[17] M. L. Boas, *Mathematical Methods in the Physical Sciences* (Wiley, 2006), 3rd ed.
[18] M. Doi and S. F. Edwards, *The theory of polymer dynamics* (Oxford University Press, New York, 1988), 1st ed.
[19] P. Jung and P. Hanggi, Phys. Rev. A **41**, 2977 (1989).
[20] M. Abramowitz and I. A. Stegun, *Handbook of Mathematical Functions* (Dover, New York, 1972), ninth ed., p.374.
[21] B. V. R. Tata and A. K. Arora, J. Phys.: Condens. Matter **7**, 3817 (1995).
[22] S. Auer, W. C. K. Poon, and D. Frenkel, Physical Review E **67**, 039904 (2003).
[23] H. F. Eicke, M. Borkovec, and B. Das-Gupta, J. Phys. Chem. **93**, 314 (1989).
[24] R. J. Hunter, *Zeta potential in colloid science: Principles and applications* (Academic Press, London, 1981).
[25] A. Kitahara, T. Satoh, S. Kawasaki, and K. Kon-No, J. Coll. Interf. Sci. **86**, 105 (1982).
[26] M. D. Croucher, K. P. Lok, R. W. Wong, S. Drappel, J. M. Duff, A. L. Pundsack, and M. L. Hair, J. Appl. Polym. Sci. **30**, 593 (1985).

VI. FIGURES

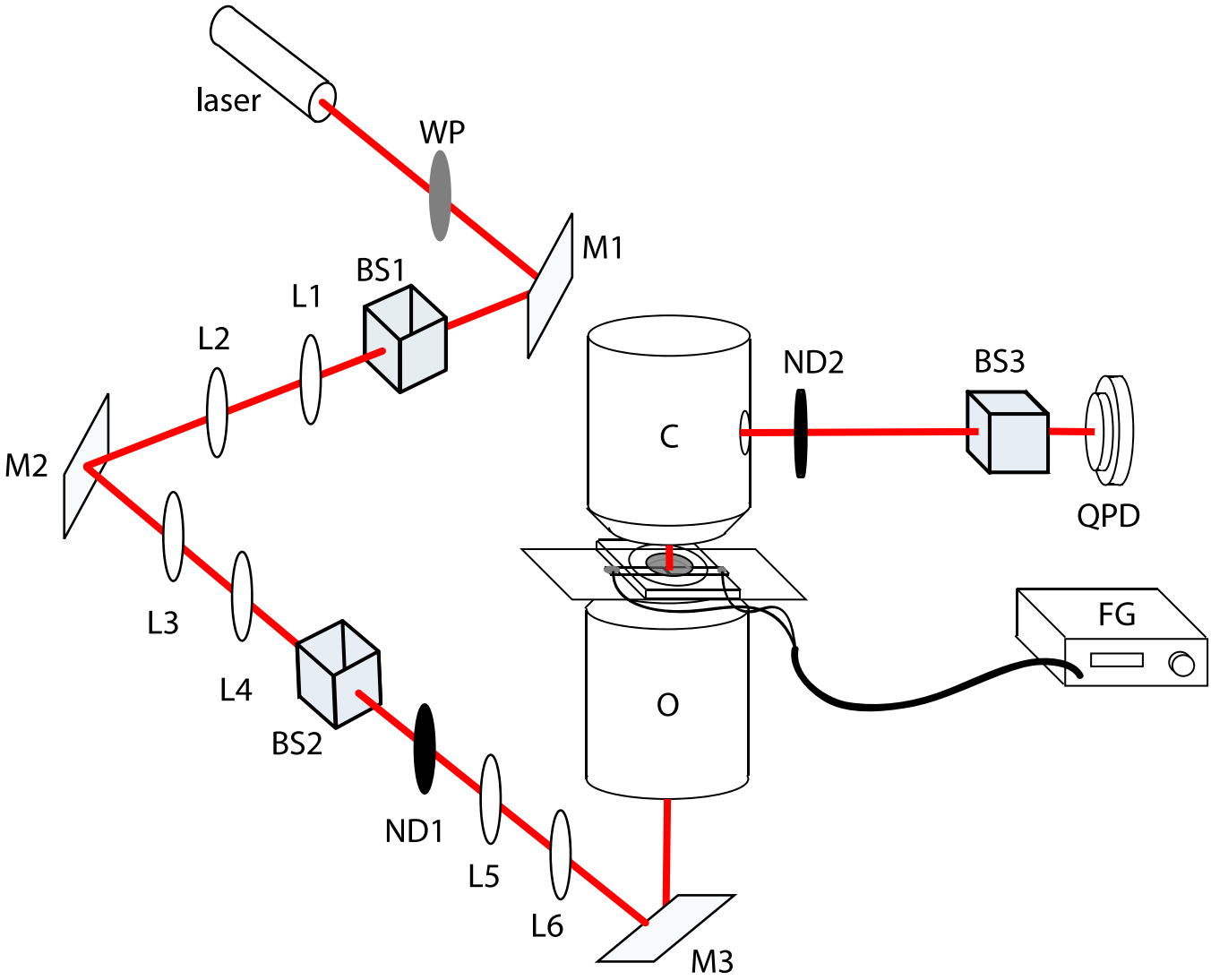

FIG. 1: Simplified experimental set-up of optical microelectrophoresis apparatus. WP, $\lambda/2$-wave plate; M, gimbal mirror; BS, beam-splitting cube; L, lens; ND, neutral density filter; O, oil-immersion objective; C, high NA-condenser; QPD, quadrant photodetector; FG, function generator.

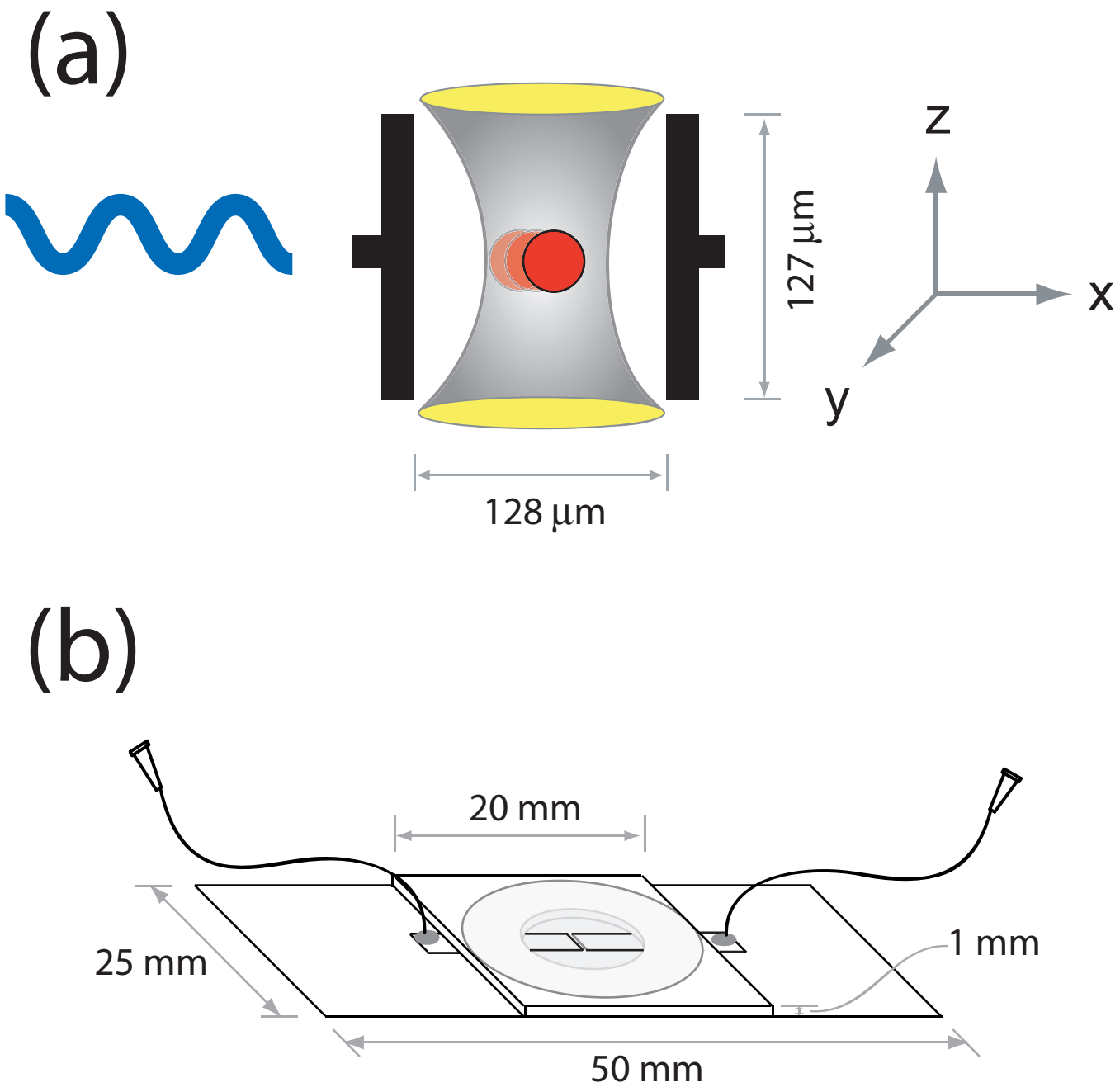

FIG. 2: (a) Experimental geometry for the optical microelectrophoresis apparatus (not to scale). (b) Optical cell.

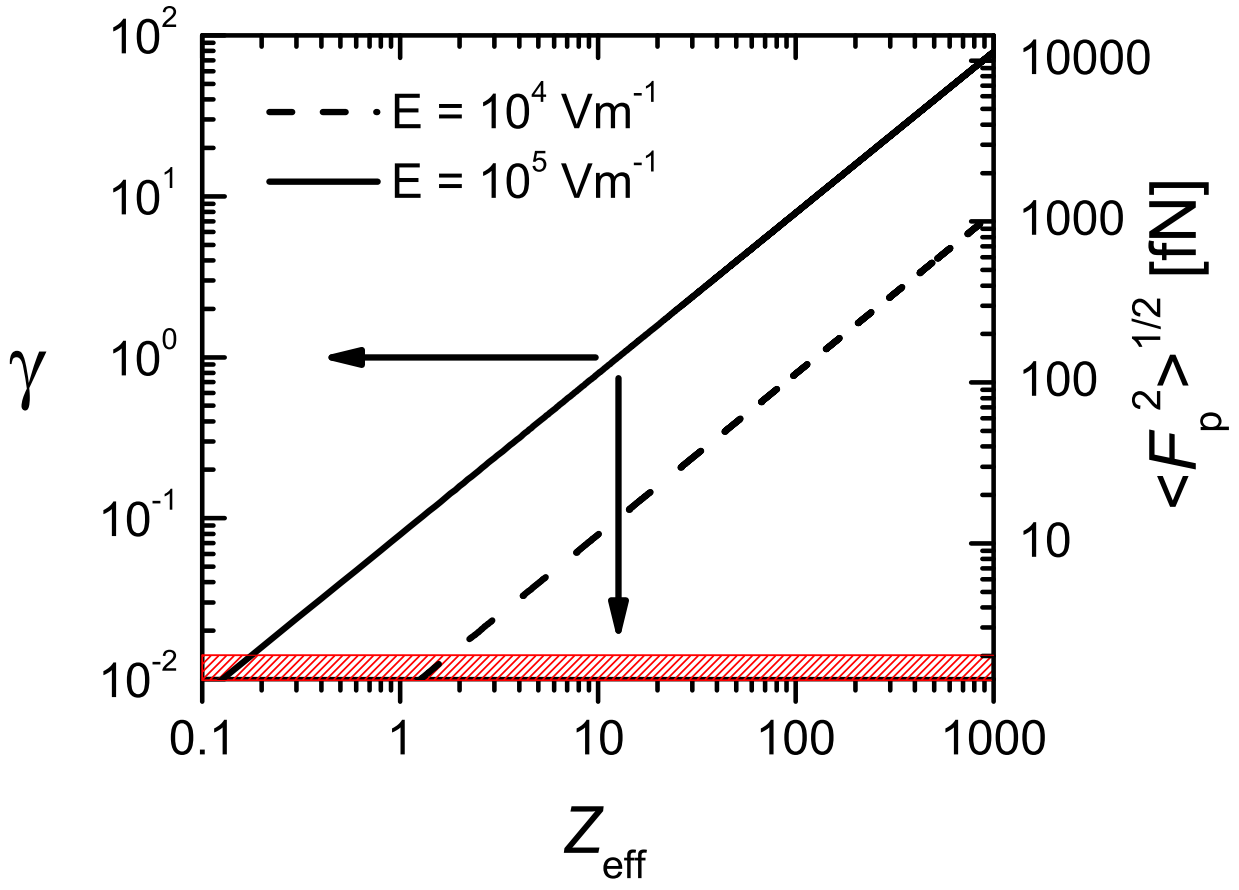

FIG. 3: The dimensionless ratio γ of electric and Brownian forces. The trapped particle has a charge $eZ_{\rm eff}$ and is placed in an oscillatory electric field of amplitude E and frequency ω_p. The Brownian forces (shown on the right-hand axis) are calculated assuming $\omega_p \ll \omega_c$ and a force constant of $k_H = 5$ fN nm^{-1}. The shaded region indicates the noise floor where the spectral density of the electric and Brownian forces are equal at ω_p. The boundary is calculated assuming $a = 500$ nm, $\eta = 1.38$ mPa s and $t_0 = 26$ s. In the shaded region, the charge on the particle is too low to be detectable by the current technique. The limiting charge sensitivity is $\sim 2\ e$ and $0.2\ e$ for fields of 10^4 and 10^5 Vm^{-1}, respectively.

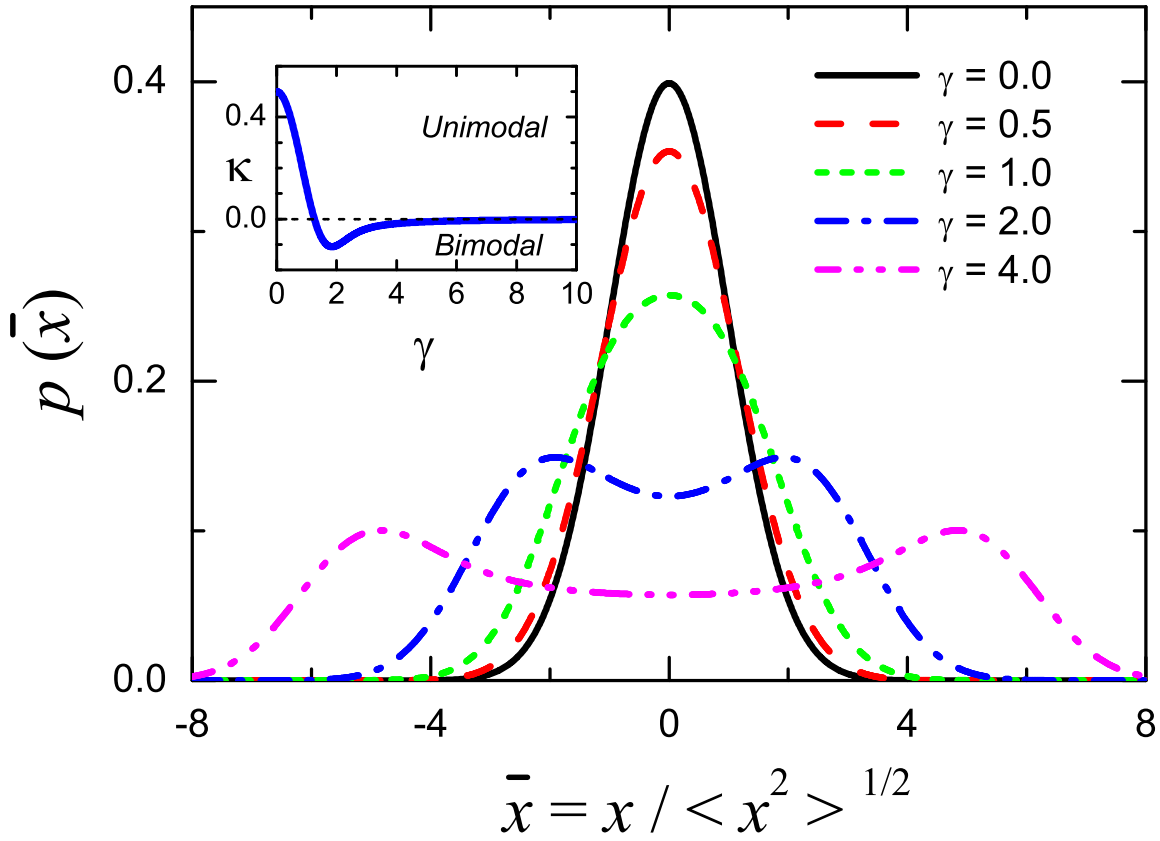

FIG. 4: The balance between thermal and electric forces. The full lines show the dependence of the asymptotic probability distribution, $p(\bar{x})$, on the ratio γ of the electric and thermal forces. The inset plot shows the curvature κ of $p(\bar{x})$, evaluated at the origin $\bar{x} = 0$. The probability distribution is double peaked for $\gamma \geq 1.257$ where κ changes sign.

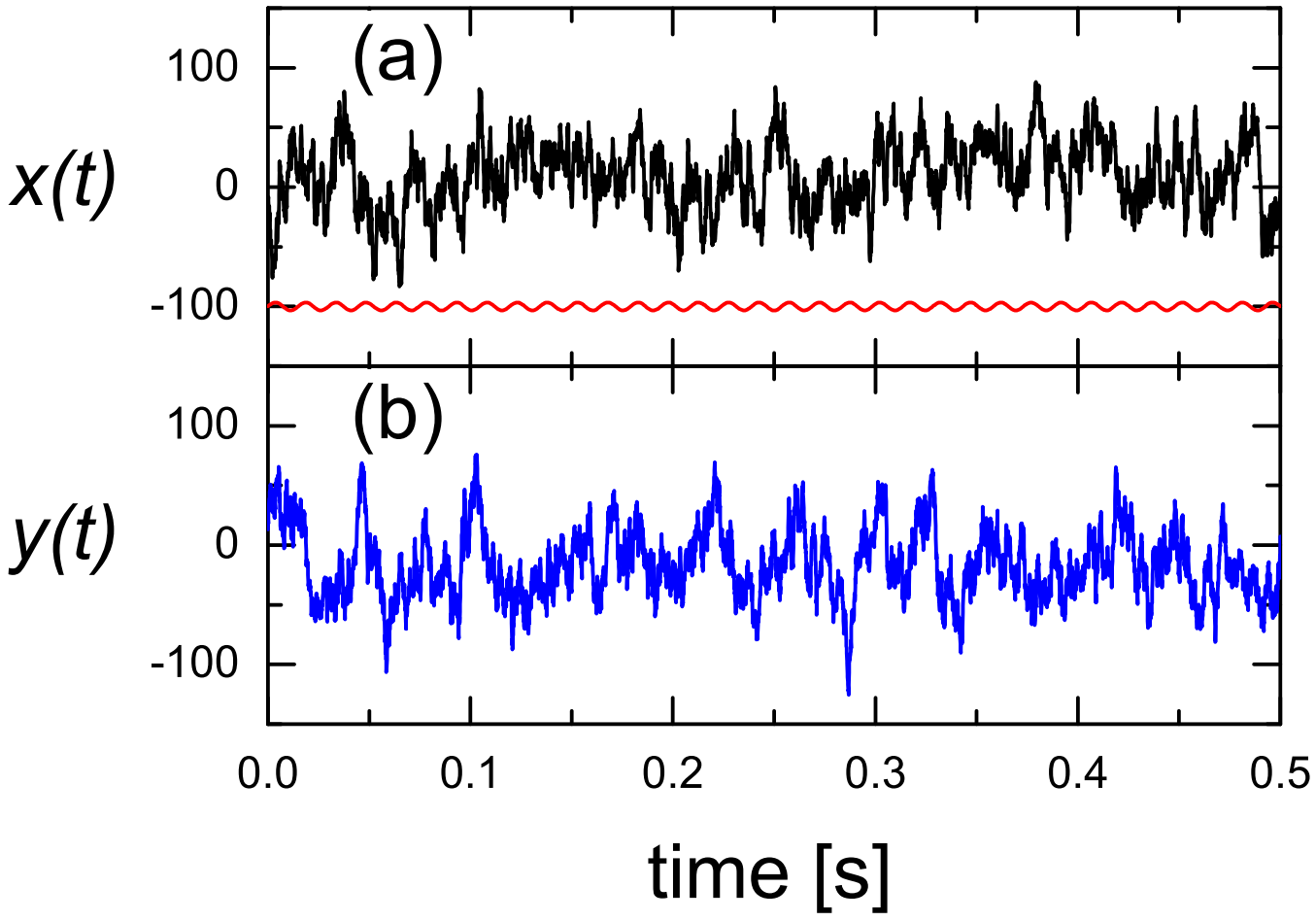

FIG. 5: Time trace of the x– and y–coordinates of a charged particle in a sinusoidal electric field. The field was aligned along the x-axis and had a frequency of 67 Hz and an amplitude of 13.3 kV m^{-1}. Periodic oscillations are not visible in the measured trajectory, which is dominated by random Brownian fluctuations. The relative size of the periodic oscillations expected are illustrated by the lower curve in (a).

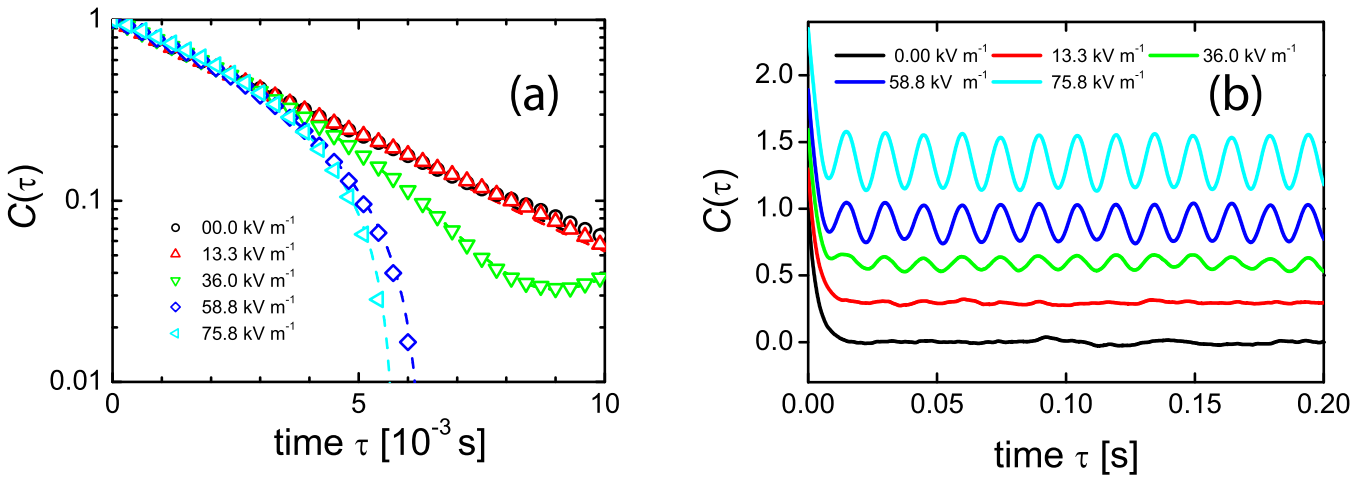

FIG. 6: The measured autocorrelation function $C(\tau)$. The sample was a PMMA particle in dodecane (containing 0.035 wt% free PHSA-g-PMMA copolymer). Data was recorded for 26 seconds at each field. The driving frequency ω_p was 420.8 rad s^{-1}. Fig. (a) shows that at short delay times the measured autocorrelations collapse to a single exponential decay. The dashed lines in (a) are least-squares fits to Eq. 14, with a corner frequency of 295 $\pm$ 7 rad s^{-1}. Fig. (b) reveals the periodic correlations found at long delay times. The curves have been vertically displaced for clarity.

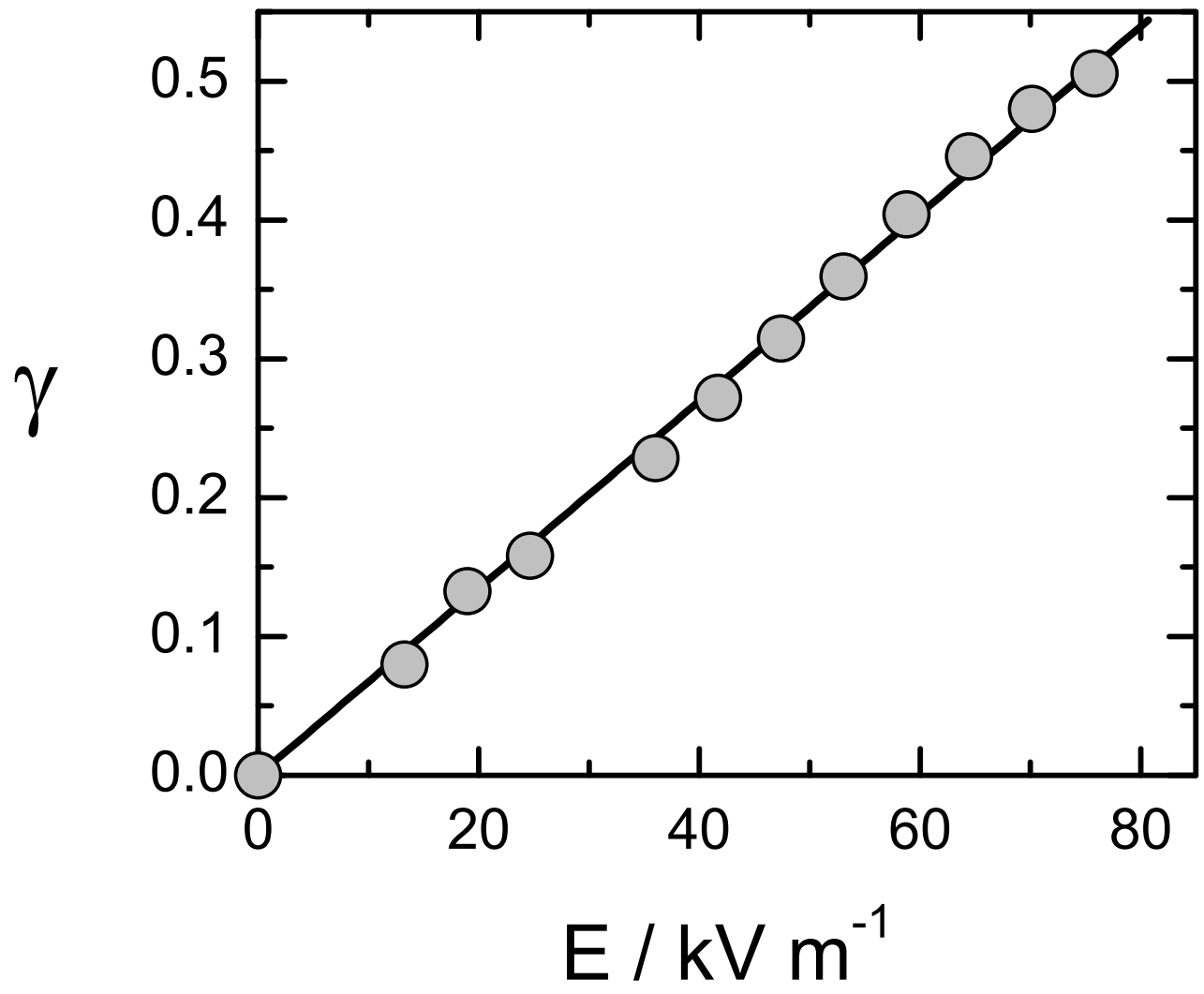

FIG. 7: The field dependence of the force ratio γ. γ was obtained by fitting the autocorrelations displayed in Fig. 6 to Eq. 14. The linear variation of γ with the field E confirms that the charge on the particle is independent of the strength of the applied field. The solid line yields an effective charge of $|Z_{\text{eff}}| = 14.5 \pm 0.2$.

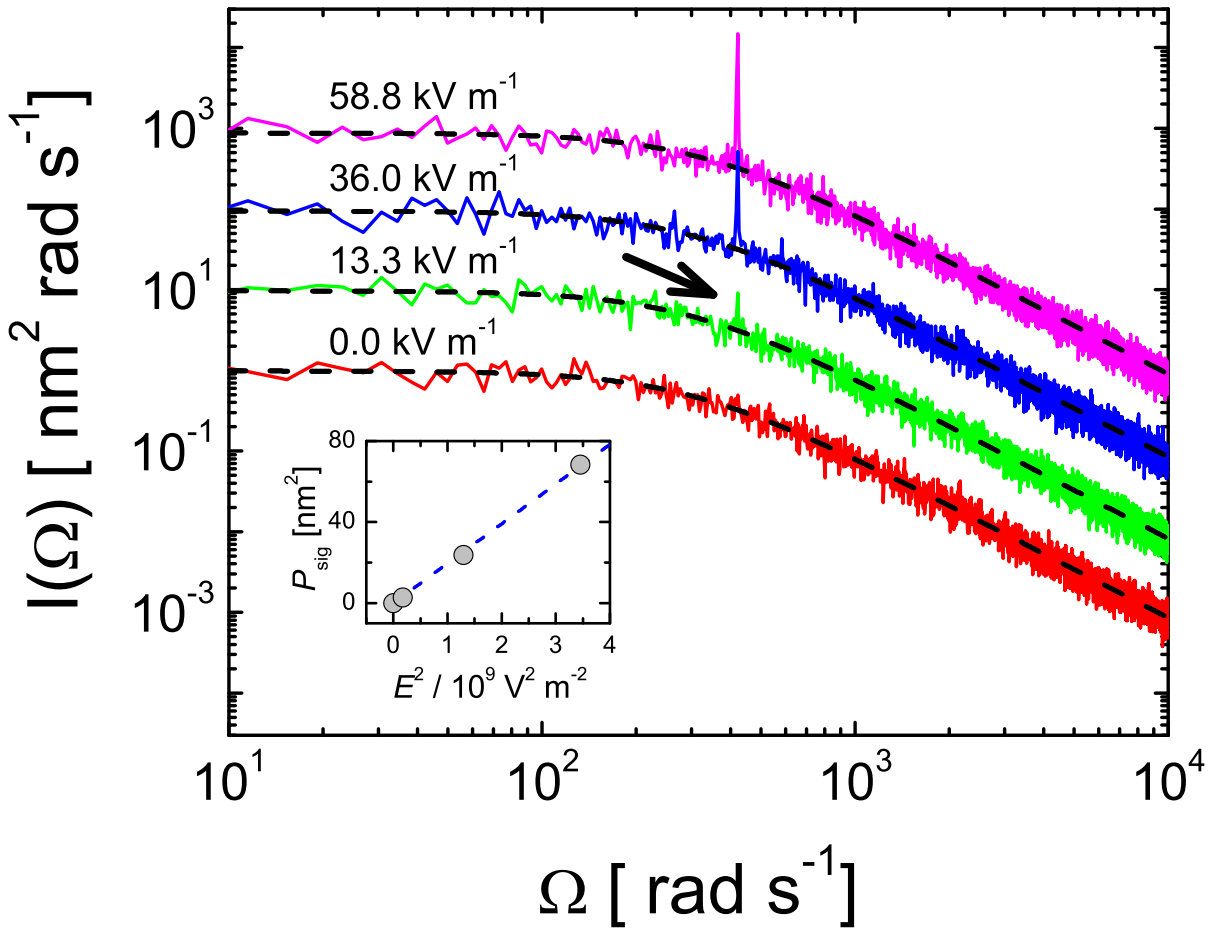

FIG. 8: The field dependence of the spectral density $I(\Omega)$. The sample was a 610 nm PMMA particle suspended in dodecane with 0.035 wt% added PHSA-g-PMMA copolymer. The variance of the power spectrum was reduced by averaging together 64 spectra, calculated from consecutive trajectories each containing 2^{14} data points ($t_0 = 1.64$ s) recorded on the same particle.

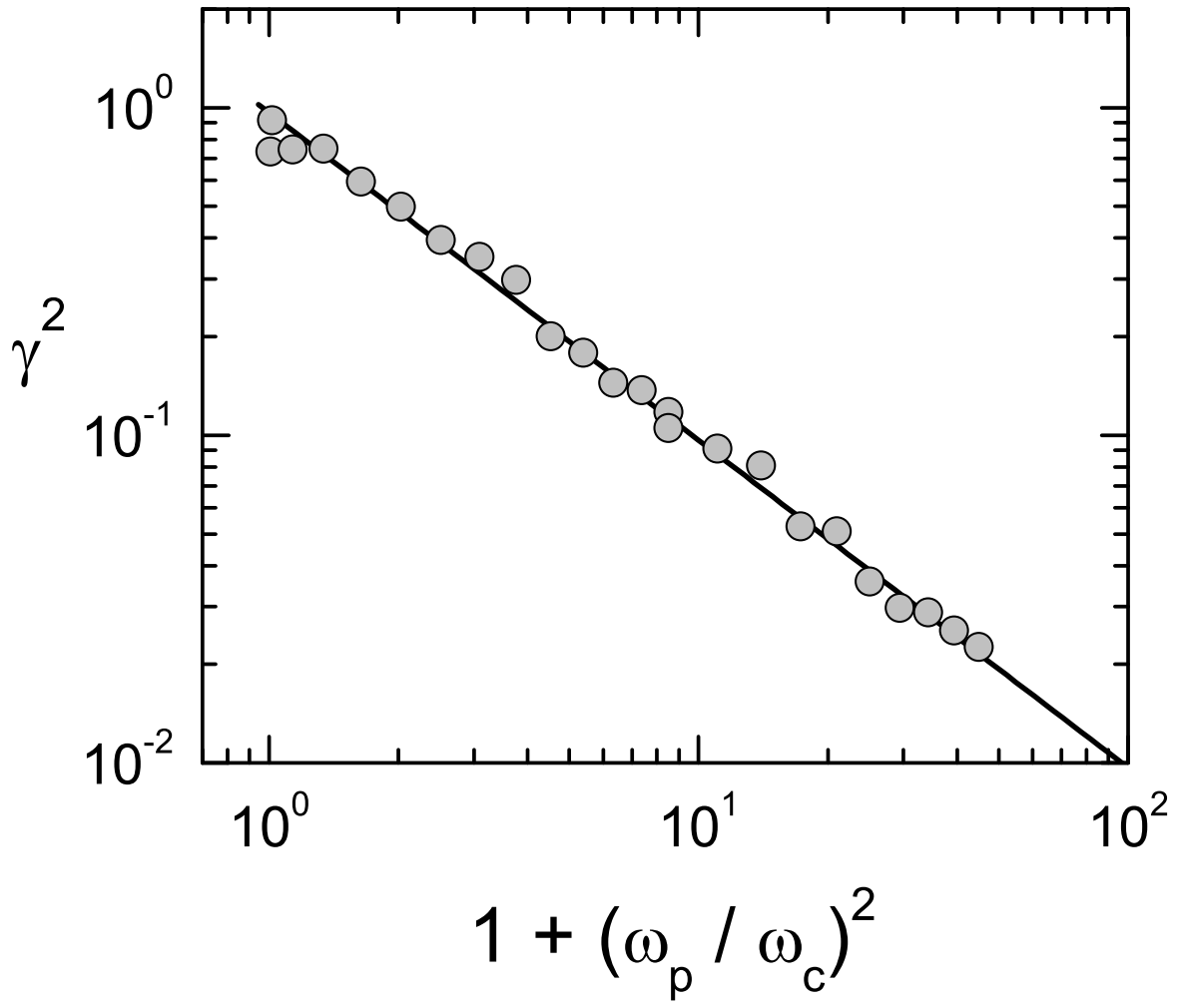

FIG. 9: The frequency dependence of the force ratio γ. The amplitude of the electric field was fixed at $E = 75.8$ kV m^{-1} and the frequency ω_p varied. The solid line is a least-squares fit of $\log \gamma^2$ against $\log(1 + (\omega_p/\omega_c)^2)$ with a gradient of -0.98 $\pm$ 0.02.

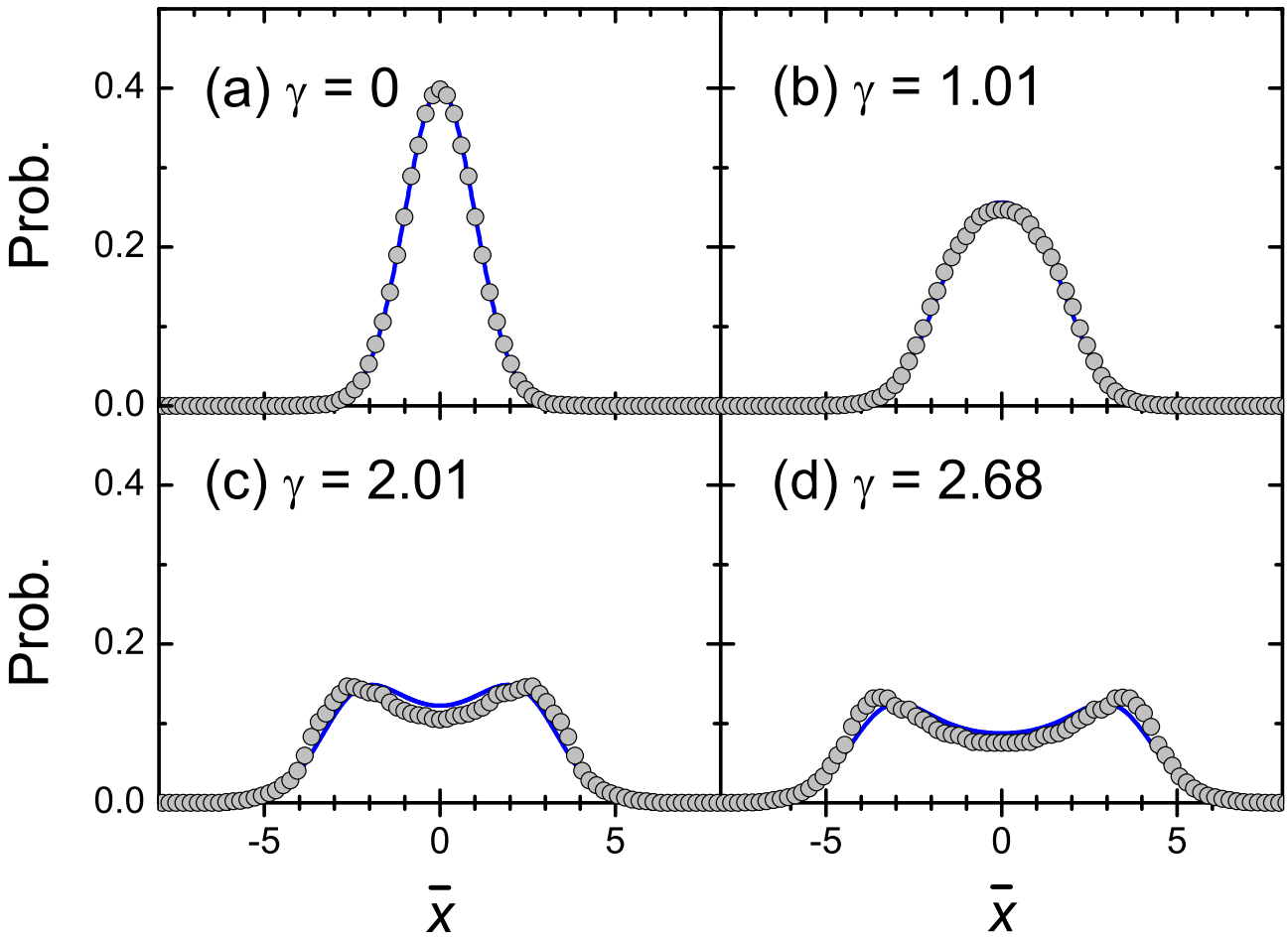

FIG. 10: The probability distributions characterising the restricted diffusion of an optically-trapped PMMA particle in a solution of 100 mM Na-AOT in dodecane. The corner frequency of the optical trap was 25.0 Hz. The points give the measured distribution in electric fields of amplitude (a) 0 kV m^{-1}, (b) 22.8 kV m^{-1}, (c) 45.5 kV m^{-1}, and (d) 60.7 kV m^{-1}. The sinusoidal electric field had a frequency of 17.5 Hz. The solid lines were calculated from the theory for a driven harmonically-bound particle (Eq. 22) using experimentally-measured parameters. The comparison has no adjustable parameters.

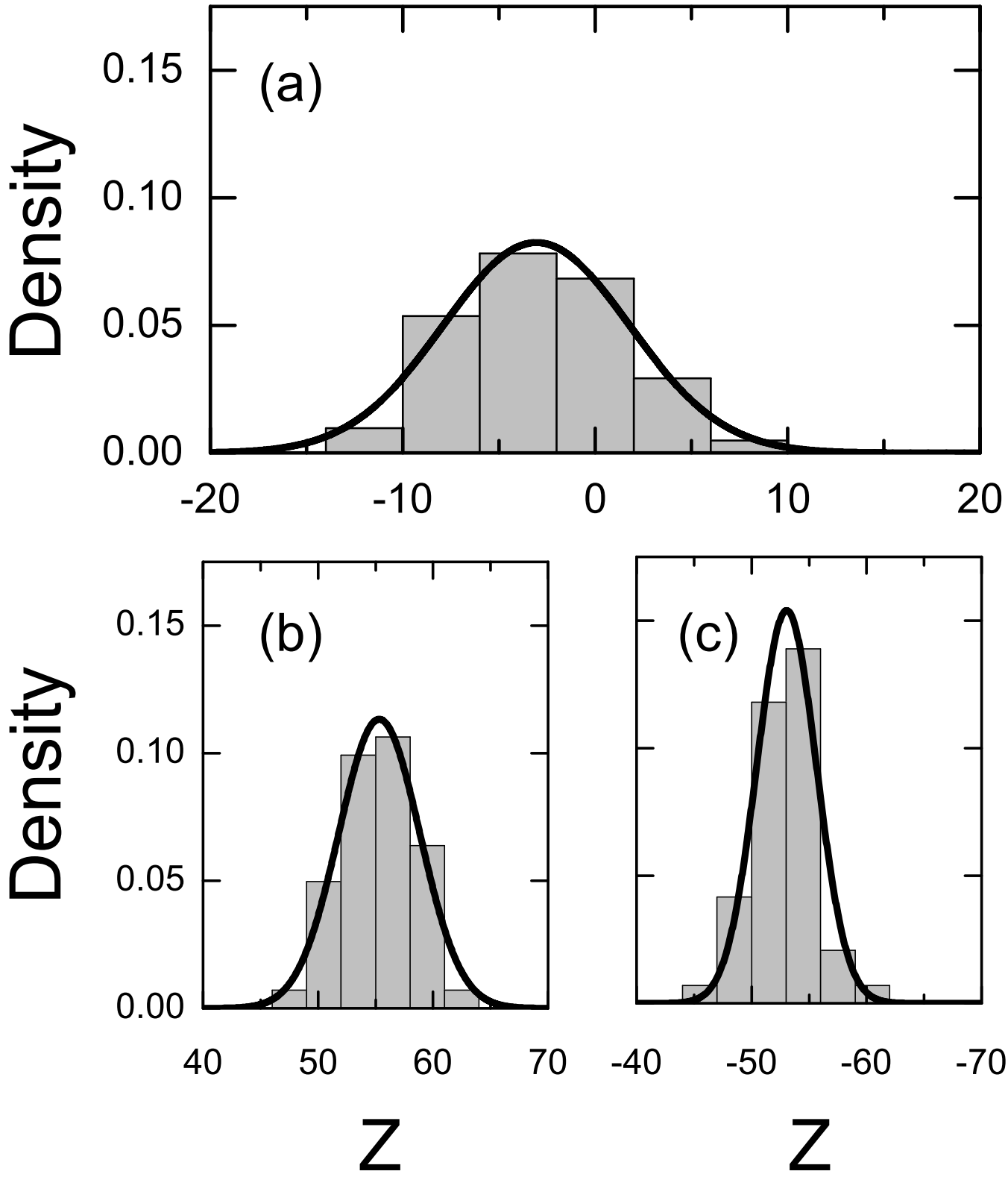

FIG. 11: The charge probability distribution measured for PMMA particles in dry dodecane with (a) no added surfactant, (b) 2 mM zirconyl 2-ethyl hexanoate, and (c) 2 mM sodium-AOT added. The full lines are Gaussian fits.